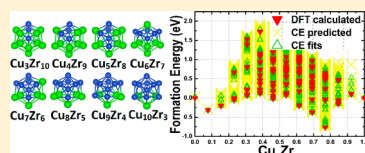


Theoretical Study on the Composition Location of the Best Glass Formers in Cu–Zr Amorphous Alloys

Da Wang,^{†,‡} Shi-Jin Zhao,^{*,†} and Li-Min Liu^{*,‡}[†]Key Laboratory of Microstructures and Institute of Materials Science, Shanghai University, Shanghai 200072, China[‡]Beijing Computational Science Research Center, Beijing 100084, China

ABSTRACT: This study combines the molecular dynamics (MD) simulations and first-principles approach to explain the experimental observation that the best glass formers of Cu–Zr bulk metallic glasses (BMGs) have the compositions $\text{Cu}_{50}\text{Zr}_{50}$ and $\text{Cu}_{64}\text{Zr}_{36}$. These two best glass formers are first calculated to be most abundantly composed of Cu_6Zr_7 and Cu_8Zr_5 icosahedral clusters when compared in the compositional range of $\text{Cu}_x\text{Zr}_{100-x}$ ($45 \leq x \leq 70$), and then these two icosahedral clusters are calculated to have the lowest formation energy among the icosahedral clusters $\text{Cu}_x\text{Zr}_{13-x}$ ($3 \leq x \leq 10$), as well as possessing some characteristics in electronic structure and chemical hardness. Through understanding the properties of specific icosahedral clusters in metallic glasses, the structural and energetic contribution to the glass-forming ability are systematically discussed.



1. INTRODUCTION

There are increasing researches on bulk metallic glasses (BMGs), which are a new class of metallic alloys with amorphous atomic structure.^{1–3} They have a variety of technologically promising properties, including high yield strength, superior elastic strain limit, good stability, and ease to process.^{4–8} BMGs are obtained by rapidly quenching the high-temperature liquid that contains several types of chemical elements. However, within the alloys composed of different relative weights of chemical elements, there is large difference in their tendency of forming glass. This tendency is generally evaluated with glass-forming ability (GFA), which describes the size of bulk volume that BMGs could achieve.^{9–11} The more the tendency of forming glass, the larger the achievable size, and the higher the GFA value.^{12–16} The composition with largest GFA value compared among all the compositional varieties of an alloy system is regarded as the best glass former. The best glass former with the largest bulk volume considerably extends the industrial applications of BMGs, and therefore it has gained the most attention of researchers in this field.

Most of the research on the best glass former is conducted to understand their physical properties, such as structural characters, thermodynamics properties, and the kinetics of the glass-forming process.^{2,17–20} There is some research now trying to explain why the experimentally determined best glass formers have a particular relative weight of their composing elements. If the chemical composition of the best glass former could be explained and predicted, it would be a considerable guidance for more effectively manufacturing the larger bulk materials of BMGs. There have been several molecular dynamics (MD) and *ab initio* MD simulations undertaken to trace the structural features of the best glass formers, to obtain some clues for explaining the compositional location.^{5,11,21–24}

The studies on some alloys have suggested that the best glass former may be characterized by the crystal/liquid interfacial structure,¹¹ specific atomic ordering in the supercooled liquid

and the amorphous state,^{5,25,26} and the interaction between the Fermi surface and the Brillouin zone in a nearly free-electron model.^{15,23} However, almost all existing theoretical studies on the correlation between physical characteristics and GFA are focused on the alloys with the best GFA determined by experiments as the premise. In principle, single-component molecular dynamics simulations seem unable to explain the compositional location of the best glass former. The reason lies in that under the widely used cooling rates from 10^9 to 10^{12} K/s, most of the compositions could have a tendency to form glass.^{11,22} For locating the composition position of the best glass former, the preliminary proposition is to comparatively study all the possible compositions of the alloy system. Until now, many studies^{27–29} on the relationship between the glass-forming ability and the compositions of BMGs have been mainly focused on the kinetic factors and the thermodynamic stability of the systems; some research on the compositional location of the best glass formers to their major orders has been recently explored.

This study aims to theoretically explain the compositional location of the best glass former from the perspective of comparative analysis, and as the first step, it focuses on the Cu–Zr alloy system as a case study. The Cu–Zr alloy has attracted much research attention, because it is one of the most easily feasible BMGs.^{1,3,11,24,30,31} Its best glass formers have been experimentally determined to be located at the compositions of $\text{Cu}_{50}\text{Zr}_{50}$ and $\text{Cu}_{64}\text{Zr}_{36}$.^{24,31,32} What makes it puzzling is that it is located particularly at these two compositions, rather than somewhere else. It is also not too close to the eutectic points,^{21,33–35} which are $\text{Cu}_{45.7}\text{Zr}_{54.3}$ and $\text{Cu}_{61.8}\text{Zr}_{38.2}$, although the glass-forming tendency is widely accepted to dramatically increase near the eutectic due to the high reduced glass

Received: December 2, 2014

Revised: December 27, 2014

Published: December 29, 2014

Table 1. Calculated Spin Multiplicity (M), Average Bond Length (d), Average Binding Energy per Atom (E_b), Vertical Ionization Potential (VIP), and Vertical Electron Affinity (VEA) for the Icosahedral Cu_{13} and Zr_{13} Clusters, Compared with the Available Experimental and Other Theoretical Results^a

cluster	M	d (Å)	E_b (eV/atom)	VIP (eV)	VEA (eV)
Cu_{13}	5 (5) ^e	2.50 (2.51) ^c	2.23 (2.19) ^e	5.52 (5.80) ^c	2.78 (2.73 ± 0.15) ^d
Zr_{13}	6 (6) ^b	2.98 (2.90) ^b	4.67 (4.48) ^e	3.74	2.14

^aThe experimental or theoretical values are shown in parentheses. ^bReference 45. ^cReference 46. ^dReference 44. ^eReference 47.

temperature, T_{rg} . Recently, Ward et al.³⁶ have proposed a general model to explain glass formation at all compositions in Cu–Zr metallic glasses; the good glass-forming abilities at $\text{Cu}_{50}\text{Zr}_{50}$ and $\text{Cu}_{64}\text{Zr}_{36}$ have been well explained by the formation of ideally packed clusters at the expense of atomic arrangements with excess or deficient free volume. Because the icosahedra and their networks were found to play an important role in slowing the dynamics and enhancing the stability in Cu–Zr glasses with ≤ 45 at. % Zr, they do not exert a unique influence on the glass-forming ability in $\text{Cu}_{50}\text{Zr}_{50}$ MGs, and this effect is shared with other clusters types as well. How these icosahedral clusters together with other efficiently packed polyhedra achieve the structure, energetics, and kinetics at a minimum, which eventually determine the formation of improved metallic glasses, remains to be further discussed.

To find the reason for the compositional location of the best glass formers in this system, we investigate the best glass former within the wide range of chemical compositions concerning the variation in the relative weight of two chemical elements. The molecular dynamics simulations are first employed to show that the whole series of $\text{Cu}_x\text{Zr}_{100-x}$ ($45 \leq x \leq 70$) alloys are dominantly composed of $\text{Cu}_x\text{Zr}_{13-x}$ ($3 \leq x \leq 10$) icosahedral clusters. To analyze the details of these icosahedral clusters, we need to determine their crystal structures at the ground state. Because the two involved elements could occupy the different atomic sites of the clusters in many different ways, the calculation requires the combination of first-principles approach with the cluster expansion (CE) method. Though part of these arrangements could be reasonably covered by first-principles total energy calculations, others would be predicted on the basis of these calculation results using the CE method. It is found that Cu_6Zr_7 and Cu_8Zr_5 icosahedral clusters have the lowest formation energies, as well as share some common specialties in chemical properties and electronic structure, suggesting that the stability of the basic orders play an important role in determining the compositional location of the best glass formers. This work aims to link the compositional location of the best glass formers to their major orders and uncovers the subtle effect of these orders on the formation of metallic glasses.

2. MODELING AND SIMULATION

Classic molecular dynamic simulations are performed on the basis of the embedded atom method (EAM) potential within the Gibbs ensemble ($N-P-T$), as implemented in the LAMMPS code.³⁷ The random configurations of $\text{Cu}_x\text{Zr}_{100-x}$ ($45 \leq x \leq 70$) alloys are prepared by randomly replacing a certain percentage ($x\%$) of Cu atoms by Zr atoms in a cubic cell box with periodic boundary conditions containing 16 000 atoms in a B2 structure. To ensure the reliability of our statistical analysis, 15 different initial configurations are used for each composition, and all analyses of the structural features are the average statistics of them. Therefore, the results of our statistical approach are sufficient to produce meaningful

structural information. The liquids of these configurations are equilibrated for 1 ns at a high temperature of 2500 K, which is sufficient for the system to become a homogeneous liquid. The time step in all the calculations is 1 fs. The systems are then rapidly quenched to the room temperature (300 K) in 100 K decrements at a cooling rate of 500 K/ns. At each temperature decrement, MD simulations were run for 200 ps to determine the atomic configurations and thermodynamic properties.

For accurate calculation of the energy and electronic properties, first-principles simulations are carried out with the VASP package, which is based on density functional theory (DFT). The projector augmented wave (PAW) approach³⁸ and the generalized gradient approximation (GGA) with a parametrized exchange–correlation functional according to PBE³⁹ are used.⁴⁰ Periodic boundary conditions are imposed in three dimensions for all the calculations. To avoid the interaction between images, a 15 Å vacuum is used for the cluster calculation. The cutoff energy for the plane wave is set to 350 eV. Because of the large supercell and cluster calculation, the Brillouin zone integration is carried out with only the Γ point. The geometry optimization is stopped until the force on each ion is smaller than 0.01 eV/Å and the total energy converges to about 10^{-5} eV. For each stable configuration, we did first a calculation in the free-spin mode. We further checked this by performing additional calculations in the fix-spin mode for the adjacent total spin states, to ensure that the obtained spin state corresponded to the most stable spin configuration. The 4004 $\text{Cu}_x\text{Zr}_{13-x}$ ($3 < x < 10$) configurations are generated by ATAT program.⁴¹ The most stable configuration of each composition is determined by the cluster expansion (CE) approach, which is a generalization of the Ising Hamiltonian.⁴² The essence of the CE is to expand the energies of $\text{Cu}_x\text{Zr}_{13-x}$ ($0 \leq x \leq 13$) configurations in terms of the occupation variable $S_m(\sigma)$ to each lattice site m of icosahedral:

$$E(\sigma) = J_0 + \sum_i J_i \hat{S}_i(\sigma) + \sum_{j < i} J_{ij} \hat{S}_i(\sigma) \hat{S}_j(\sigma) + \sum_{k < j < i} J_{ijk} \hat{S}_i(\sigma) \hat{S}_j(\sigma) \hat{S}_k(\sigma) + \dots \quad (1)$$

We define $S_m(\sigma)$ as +1 when site m is occupied by a Cu atom and -1 if it is occupied by Zr. The coefficients J_α in eq 1 are called the effective cluster interaction (ECI),⁴³ which is independent of $S_m(\sigma)$. It embodies the information regarding the energetics of the $\text{Cu}_x\text{Zr}_{13-x}$ homotops. The unknown J_α can be confirmed by fitting $E(\sigma)$ to the energies of some selected homotops obtained from first-principles computations.

To check the accuracy of our computational setups, the properties of icosahedral Cu_{13} and Zr_{13} are calculated. The results are summarized in Table 1. The good agreement between the experimental (or theoretical) values^{44–47} and our results illustrates the accuracy of the present theoretical calculations.

3. RESULTS AND DISCUSSION

3.1. Microstructural Characterizations of Cu–Zr Alloys. To assess the chemical short-range order in the glassy structure, the local atomic environments of Cu–Zr BMGs are analyzed using the Voronoi tessellation method⁴⁸ analysis in terms of the Voronoi index $\langle n_3, n_4, n_5, n_6 \rangle$, where n_i denotes the number of i -edge faces of the Voronoi polyhedra (VP). In addition to the local geometry, the Voronoi index also defines the coordination number (CN) around an atom as $\text{CN} = \sum n_i$. Here, the histograms of the CN of Cu-centered clusters for six selected composition Cu–Zr alloys are shown Figure 1. It is

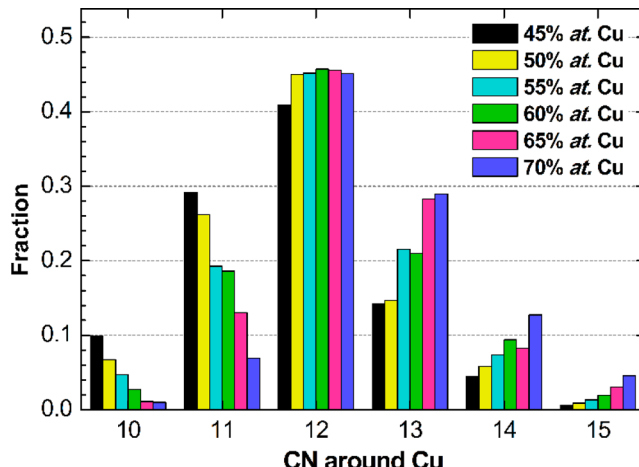


Figure 1. Total fractions of polyhedra with different CNs around Cu atoms for six different composition Cu–Zr alloys.

clear that polyhedra with $\text{CN} = 12$ are dominant in all the widely covered $\text{Cu}_x\text{Zr}_{100-x}$ ($45 \leq x \leq 70$) alloys. For further characterization of the topological short-range order (TSRO) of each composition, the fraction of these $\text{CN} = 12$ polyhedra with respect to the total number of Cu atoms was explored, as shown in Figure 2a. It is noted that with the growth of the Cu content, the proportion of $\text{CN} = 12$ dominated polyhedra gradually increased, indicating the strong response of these basic polyhedra to the compositional variation in Cu–Zr alloys. Most importantly, certain peaks show up at $\text{Cu}_{50}\text{Zr}_{50}$ and $\text{Cu}_{64}\text{Zr}_{36}$, coinciding with GFA enhanced compositions according to previously reported experimental and simulation results.^{24,31,32} The good match between the two distinguished compositional locations and GFA improvement indicate the important role of the structural factor in determining the ease of glass formation. Thus, it is significant to explore the details about these dominated polyhedral clusters.

In Figure 2b we show the detailed $\text{CN} = 12$ polyhedral clusters vary with the chemical composition. Although there are large varieties of Voronoi polyhedra, only a few of them emerge with noticeable abundance. Thus, we depict the four most frequent ones in the compositional ranges. It shows that the peaks at $\text{Cu}_{50}\text{Zr}_{50}$ and $\text{Cu}_{64}\text{Zr}_{36}$ in Figure 2a are mainly contributed by full icosahedra with a Voronoi index of $\langle 0, 0, 12, 0 \rangle$, and the trend is obviously that full icosahedra clusters exhibit the most pronounced rise, relative to the other competing Cu-centered distorted icosahedra (e.g., Voronoi index $\langle 0, 2, 8, 2 \rangle$, $\langle 0, 3, 6, 3 \rangle$, and $\langle 0, 4, 4, 4 \rangle$). Previous studies^{5,49} revealed that stable Cu-centered full icosahedra (FI) is a key structural motif in amorphous Cu–Zr alloys. These FI units have been proven to impact the dynamics of Zr–Cu glass-

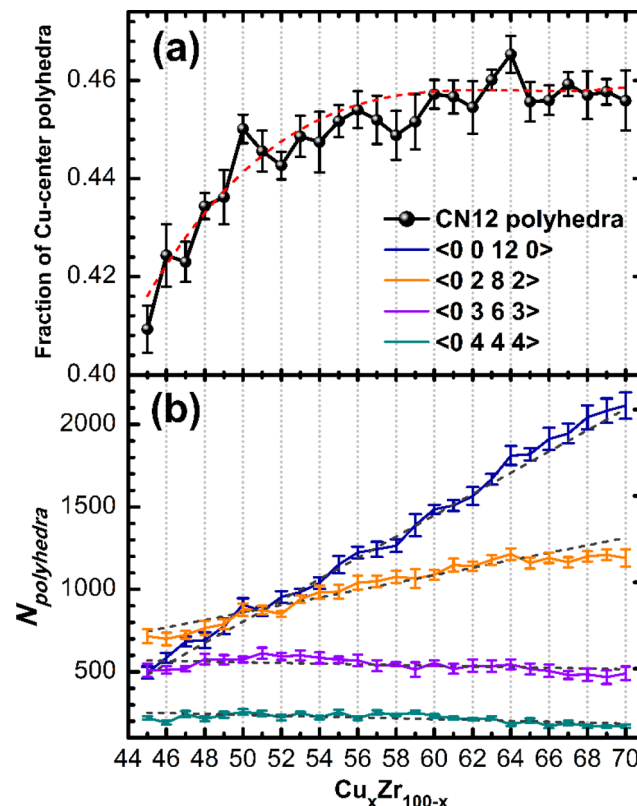


Figure 2. Voronoi polyhedral analysis around Cu atoms for different Cu–Zr compositions: (a) the fraction of $\text{CN} = 12$ polyhedra and (b) the number of four most popular types of Voronoi polyhedra.

forming liquids significantly, which makes crystallization processes more difficult and benefits the GFA.^{30,31} Here, from the statistical analysis, it is possible that the icosahedra can be a basis of beneficial structural order for the formation of metallic glasses in the Cu–Zr system. Even though these icosahedral clusters at various compositions are similar from the topological viewpoint, they should not be treated as identical clusters in the physical or chemical sense. For this purpose, we expected to find out how the chemical makeup of these icosahedra clusters change with the Cu concentration, as well as their energetic and structural contribution to glass stability.

In Figure 3, we analyze all the different icosahedron-like clusters around Cu atoms whose average numbers (N_{ico}) had ever been larger than 100 over the compositional range from $\text{Cu}_{45}\text{Zr}_{55}$ to $\text{Cu}_{70}\text{Zr}_{30}$. It is shown that the Cu:Zr ratio of the dominant clusters change from 6:7 to 9:4, and the changing curve of Cu_6Zr_7 , Cu_7Zr_6 , and Cu_8Zr_5 clusters are seen as a downward parabola with a maximum near $\text{Cu}_{50}\text{Zr}_{50}$, $\text{Cu}_{57}\text{Zr}_{43}$, and $\text{Cu}_{64}\text{Zr}_{36}$, respectively. In addition, the Cu_6Zr_7 and Cu_8Zr_5 clusters dominated significantly larger compositional range than other types, viz., 10% in range from $\text{Cu}_{45}\text{Zr}_{55}$ to $\text{Cu}_{54}\text{Zr}_{46}$ for Cu_6Zr_7 and 9% in range from $\text{Cu}_{60}\text{Zr}_{40}$ to $\text{Cu}_{68}\text{Zr}_{32}$ for Cu_8Zr_5 , respectively, which compared to only 5% in range from $\text{Cu}_{55}\text{Zr}_{45}$ to $\text{Cu}_{59}\text{Zr}_{41}$ for Cu_7Zr_6 . This indicates that the Cu_6Zr_7 and Cu_8Zr_5 clusters are more stable. More importantly, the N_{ico} peaks of Cu_6Zr_7 and Cu_8Zr_5 clusters at $\text{Cu}_{50}\text{Zr}_{50}$ and $\text{Cu}_{64}\text{Zr}_{36}$, respectively, are consistent with the peak positions shown in Figure 2. In fact, the Cu-centered Cu_6Zr_7 and Cu_8Zr_5 icosahedral clusters have been identified as the basic clusters of $\text{Cu}_{50}\text{Zr}_{50}$ and $\text{Cu}_{64.5}\text{Zr}_{35.5}$ MGs in both the experimental measurements and molecular dynamics simulations,^{25,30,31,50–52}

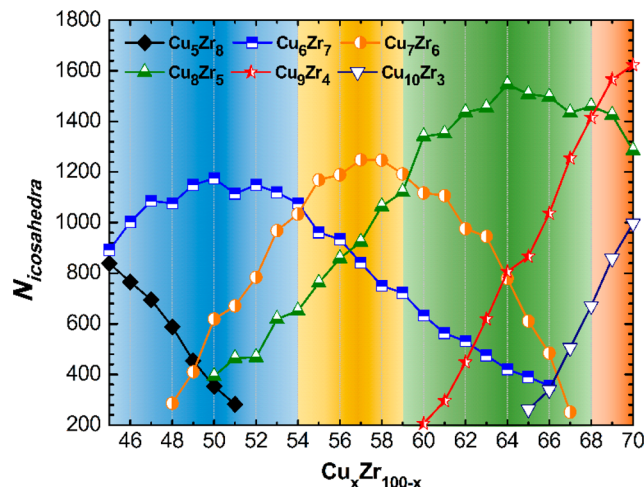


Figure 3. Average numbers of the most popular icosahedral-like clusters (N_{ico}) around Cu atoms over the compositional range from $\text{Cu}_{45}\text{Zr}_{55}$ to $\text{Cu}_{70}\text{Zr}_{30}$.

and the corresponding compositions with the best GFA can be described as an “ICO + glue atom” arrangement, viz., $\text{Cu}_{50}\text{Zr}_{50} = \text{Cu}_6\text{Zr}_7 + \text{Cu}$ and $\text{Cu}_{64.3}\text{Zr}_{35.7} = \text{Cu}_8\text{Zr}_5 + \text{Cu}$.^{25,51} In our study, the links between the glass formation and the characteristic structures in metallic glasses were identified. Because the energetics and kinetics are closely dependent on the ideally packed structure in metallic glasses, we expect to further understand the compositional location of the best glass former by exploring the nature of the local structures in the system.

3.2. Crystal Structure and Stability of $\text{Cu}_x\text{Zr}_{13-x}$ Clusters ($x = 3-10$). It has been known that the icosahedra in the metallic glasses coexist with other low-energy polyhedrons to minimize the local energy density by forming the densest atomic packing. However, due to the lack of understanding of the structural features of local icosahedral order and their correlation with the long-range disorder in BMGs, it is hard to discuss the properties of these specific icosahedral configuration effects on GFA combined with their surrounding atomic environment. Nevertheless, one conclusive discovery in our current study is that those icosahedral clusters with the dominant population and stable structure play a crucial role in determining the compositional location of the best glass former. For this purpose, we try to explore the effect of the local icosahedral clusters on GFA in Cu–Zr alloy system by considering these icosahedral clusters independently. It is reasonable because for the same topological icosahedral short-range orders (ISRO), they are located in a similar coordination environment for the dense packing from the statistical point of view. As the influence of their surrounding coordinating atoms are offset, it would be an efficient way to identify the basic properties of the icosahedral clusters to understand the intrinsic relation between the localized atomic orderings and GFA. However, due to the extremely large number of the $\text{Cu}_x\text{Zr}_{13-x}$ icosahedral configurations, because the shell is composed of Cu and Zr atoms, few reports about the certain arrangement of icosahedral clusters have been systematically discussed so far. In our work, all the possible atomic configurations of Cu-centered $\text{Cu}_x\text{Zr}_{13-x}$ ($x = 0-13$) icosahedral clusters in Cu–Zr metallic glass are examined by first-principles calculations combined with the cluster expansion (CE) approach. We aim to explain the compositional location of the best glass formers on the basis

of the nature of the basic icosahedral units in Cu–Zr BMGs. Accordingly, the ground state geometry of $\text{Cu}_x\text{Zr}_{13-x}$ ($x = 3-10$) icosahedral polyhedra are determined first. Due to the large number of possible structural forms of inhomogeneous clusters, we have used the term “homotops”, introduced by Jellinek and co-workers,^{53,54} to describe A_mB_n alloy clusters with a fixed number of atoms ($N = m + n$) for a defined composition (m/n ratio). Without point group symmetry, a single geometry of an N -atom AB cluster have homotops

$$N_{P_{A,B}} = \frac{N!}{N_A!N_B!} = \frac{N!}{N_A!(N - N_A)!} \quad (2)$$

where N_A and N_B are the number of atoms of type A and type B, respectively, and N is the total number of atoms. The total quantity of homotops with any composition for a given structure is 2^N , which is approximately 4×10^3 for Cu-centered $\text{Cu}_x\text{Zr}_{13-x}$ ($x = 3-10$) clusters. Due to the extremely small energy difference between homotops (less than 0.01 eV in our case), the traditional empirical force field calculations cannot meet the prediction accuracy for structural energies. On the contrary, density functional theory (DFT) calculation has been widely employed to determine the exact energy of various substances, whereas it is rather expensive to calculate all 4004 kinds of configurations. To solve this problem, the cluster expansion (CE) approach, as described in detail in Modeling and Simulation, was used to search the most stable configurations among a variety of $\text{Cu}_x\text{Zr}_{13-x}$ arrangements on the basis of the DFT calculations. By this approach, all of the 4004 energies of $\text{Cu}_x\text{Zr}_{13-x}$ homotops are predicted by calculating some parts of them (about 20%) from DFT.

In our calculations, the cross-validation (CV) score⁵⁵ is designed to evaluate the predictive power of a cluster expansion, which is defined as

$$(CV)^2 = n^{-1} \sum_{i=1}^n (E_i - \hat{E}_{(i)})^2 \quad (3)$$

where E_i and $\hat{E}_{(i)}$ are the calculated and predicted energies of structure i , respectively. It is small enough (0.091 eV/fu) to ensure the accuracy of the calculations after the energies of up to 893 $\text{Cu}_x\text{Zr}_{13-x}$ ($3 \leq x \leq 10$) homotops are finally calculated by first principles. On the basis of J_α obtained by fitting the energies of 893 homotops, the energy dependence of the 4004 Cu–Zr homotops are evaluated by cluster expansion. As shown in Figure 4, the formation energies calculated by first-principles (red filled triangles) are rather consistent with the corresponding cluster expansions ones (green hollow triangles). The root-mean-square (rms) error between 4004 CE predicted values and 893 PBE energies is 0.078 eV/fu, indicating a high reliability of our CE simulations. All the lowest energy structures and their main physicochemical properties for mixed $\text{Cu}_x\text{Zr}_{13-x}$ ($x = 3-10$) clusters are presented in Figure 5 and Table 2.

Thermodynamic analysis is an effective way to evaluate the composition of a good glass former. Inoue and co-workers proposed a thermodynamic model to determine glass-forming compositions from empirical rules.^{56,57} They calculated the mixing enthalpy (ΔH) and mismatch entropy (S_σ) of glass-forming alloys. Here the excess energy (E_{excess}) is discussed to assess the relative stability of particular stoichiometries, which is calculated by the following equation:

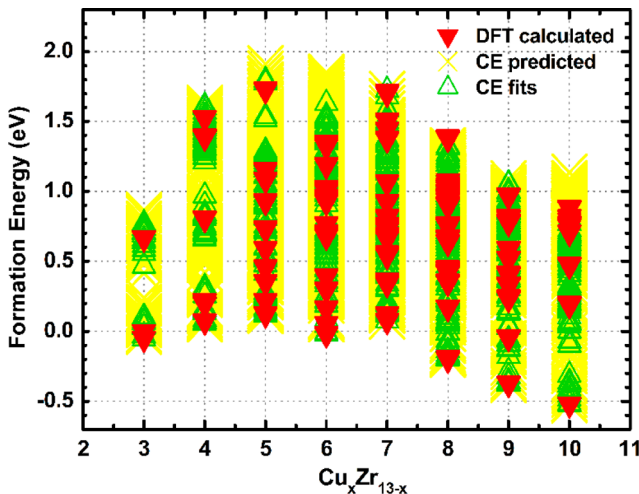


Figure 4. Formation energies (ΔE_x) of the various configurations calculated from first-principles along with the corresponding cluster expansions (CEs) fit as a function of Cu content of the inverse $\text{Cu}_x\text{Zr}_{13-x}$. The ΔE_x values of 4004 configurations calculated from CE are also plotted here. Those with formation energy larger than 2.25 eV/fu are not shown in the figure.

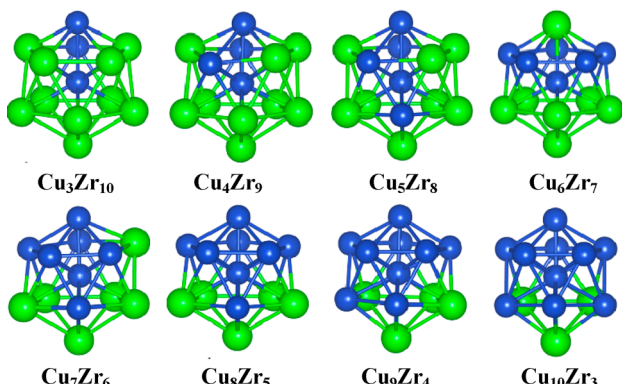


Figure 5. Ground state geometries for $\text{Cu}_x\text{Zr}_{13-x}$ for $x = 3-10$. Navy and green spheres are Cu and Zr atoms, respectively.

Table 2. Excess Energy (E), Stability Function ($\Delta_2 E$), Multiplicity (M), Vertical Ionization Potential (VIP), Vertical Electron Affinities (VEA), and Chemical Hardness (η) for the Most Stable $\text{Cu}_x\text{Zr}_{13-x}$ ($x = 3-10$) Clusters

x	E (eV)	$\Delta_2 E$ (eV)	M (μ_B)	VIP (eV)	VEA (eV)	η (eV)
3	-0.056	0.029	4	4.032	2.142	1.890
4	0.067	0.069	3	4.075	2.124	1.951
5	0.121	0.189	3	4.129	2.112	2.017
6	-0.014	-0.225	0	4.250	2.134	2.115
7	0.076	0.386	4	4.319	2.271	2.048
8	-0.220	-0.180	2	4.409	2.245	2.164
9	-0.336	0.053	4	4.556	2.415	2.141
10	-0.505	-0.534	3	4.796	2.424	2.372

$$E_{\text{excess}}(\text{Cu}_x\text{Zr}_{13-x}) = E_b(\text{Cu}_x\text{Zr}_{13-x}) - x \frac{E_b(\text{Cu}_{13})}{13} - (1-x) \frac{E_b(\text{Zr}_{13})}{13} \quad (4)$$

where $E_b(\text{Cu}_x\text{Zr}_{13-x})$ is the energy difference between the specific cluster configuration $\text{Cu}_x\text{Zr}_{13-x}$ and separated atoms

$x\text{Cu} + (13-x)\text{Zr}$. A negative value of E_{excess} , as shown in the shaded portion of Figure 6, indicates in general that mixing is

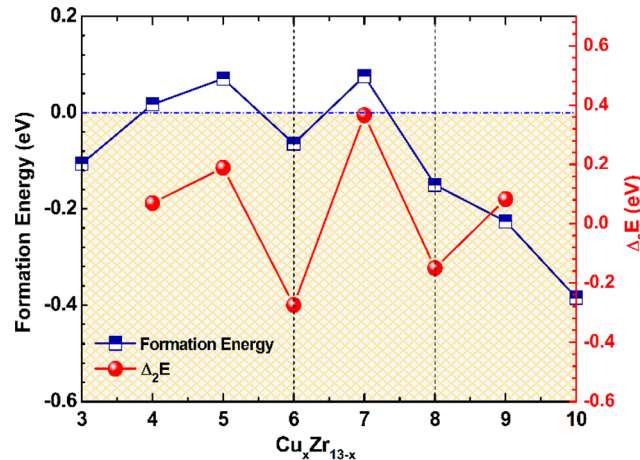


Figure 6. Excess energies, E_{excess} (navy square), and stability functions, $\Delta_2 E$ (orange circle), defined in eqs 4 and 5 for lowest energy $\text{Cu}_x\text{Zr}_{13-x}$ clusters with $3 \leq x \leq 10$.

favorable. It shows that E_{excess} presents an oscillation tendency over the composition, suggesting the existence of the particularly stable clusters. Here, stability functions ($\Delta_2 E$) are used to characterize them, which can be defined by the following equation:

$$\Delta_2 E(A_m B_n) = 2E(A_m B_n) - E(A_{m+1} B_{n-1}) - E(A_{m-1} B_{n+1}) \quad (5)$$

The clusters that have minimum $\Delta_2 E$ are supposed to be more stable than others. Figure 6 depicts the stability function ($\Delta_2 E$) for $\text{Cu}_x\text{Zr}_{13-x}$ versus the number of Cu atoms (x). Both E_{excess} and $\Delta_2 E$ show two marked valleys for $x = 6$ and 8 , indicating that these two stoichiometries are specially stable ones. As previously analyzed in section 3.1, the Cu_6Zr_7 and Cu_8Zr_5 polyhedral clusters were selected as the basic units for the formation of $\text{Cu}_{50}\text{Zr}_{50}$ and $\text{Cu}_{64}\text{Zr}_{36}$ BMGs. Here, on the basis of first-principles simulations, we suggested that the energy stability of local icosahedral orders play a fundamental role in determining the glass formation of metallic glasses.

3.3. Relationship between Electronic Structure and GFA. As the stability of the basic $\text{Cu}_x\text{Zr}_{13-x}$ icosahedron orders in Cu–Zr BMGs have been already discussed, it provides a unique opportunity to understand the effect of the electronic structure of icosahedron clusters on GFA. Here, the s-, p-, and d-projected partial density of states and total spin density [$\rho_\uparrow(\mathbf{r}) - \rho_\downarrow(\mathbf{r})$] isosurface of $\text{Cu}_x\text{Zr}_{13-x}$ clusters for $x = 4, 6, 8$, and 13 are first calculated, as shown in Figure 7. It turns out that the Cu–Zr bonding is mainly through d–d orbital hybridizations, with a limited contribution of the sp hybrid orbitals. This result is in line with previous electronic structure calculations focused on the bonding types of this kind of BMG.^{30,58–60} In addition, magnetic transfers have been found in these icosahedral clusters. For example, in Figure 7, Cu_8Zr_5 and Cu_{13} are ferromagnetic, and Cu_6Zr_7 and Cu_4Zr_9 are paramagnetic and antiferromagnetic, respectively. Notably, the significantly reduced magnetic can be observed in Cu_6Zr_7 and Cu_8Zr_5 , as shown in Table 2. These results suggest that atomic arrangements in $\text{Cu}_x\text{Zr}_{13-x}$ clusters are greatly affected by their electronic shell structures, which also determine the stability of these icosahedral configurations.

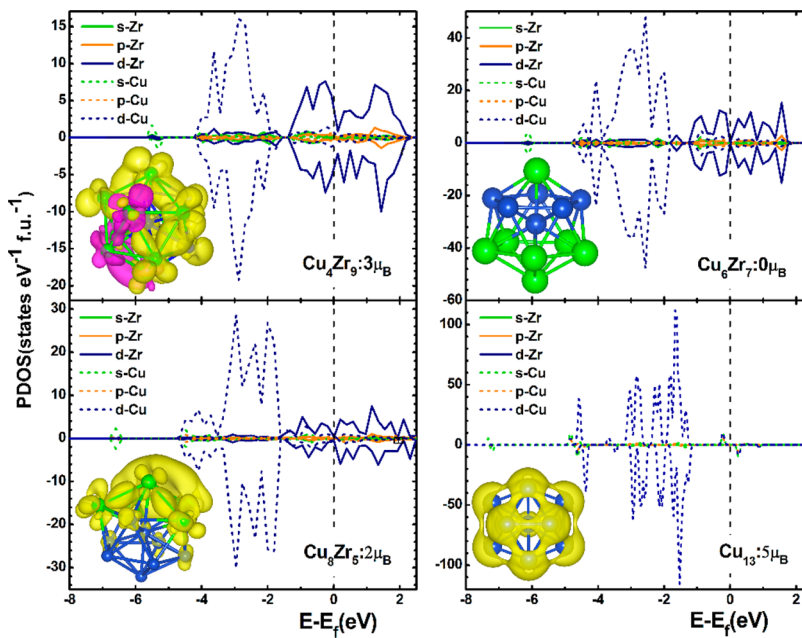


Figure 7. s-, p-, and d-projected partial density of states and total spin density [$\rho_{\uparrow}(r) - \rho_{\downarrow}(r)$] isosurface calculated for the lowest energy structure of representative Cu_xZr_{13-x} clusters with $x = 4, 6, 8$, and 13. The Fermi level is shifted to zero. The numerical numbers close to the structures are the atomic spin in units of μ_B . The purple and yellow denote an excess of minority and majority spin, respectively. To make the plot clear, the isovalues are defined as 0.0015, 0.001, 0.003, and 0.0035 au for Cu₄Zr₉, Cu₆Zr₇, Cu₈Zr₅, and Cu₁₃, respectively.

Experimentally, the electronic structure of a system is probed via measurements of ionization potentials, electron affinities, polarizabilities, etc. The vertical electron affinity (VEA) and vertical ionization potential (VIP) can be defined as

$$\text{VIP}_x = E(\text{Cu}_x\text{Zr}_{13-x}^+) - E(\text{Cu}_x\text{Zr}_{13-x})$$

and

$$\text{VEA}_x = E(\text{Cu}_x\text{Zr}_{13-x}^-) - E(\text{Cu}_x\text{Zr}_{13-x})$$

where $E(\text{Cu}_x\text{Zr}_{13-x}^+)$ (or $E(\text{Cu}_x\text{Zr}_{13-x}^-)$) represents the energies of cationic (or anionic) Cu_xZr_{13-x} clusters calculated with optimized neutral geometry, respectively. It can be seen from Figure 8 that both VIP and VEA increase as the content of Cu increases. This may not be a surprise because of the strong

electronegativity of Cu compared to that of Zr. Besides, both the VIP and VEA curves present an uneven increase, indicating the existence of the relatively stable clusters. Here, the chemical hardness η is used to further characterize the relative stability of Cu_xZr_{13-x} clusters according to the principle of maximum hardness (PMH).^{61,62} On the basis of Koopmans' theorem and finite difference approximation,⁶³ η is defined by the following equation:

$$\eta = \text{VIP} - \text{VEA}$$

It can be seen from Figure 8 that the hardness (η) of the lowest-energy Cu_xZr_{13-x} is more independent for small concentrations of Cu atoms and becomes an obvious odd-even oscillation with $x > 6$. Through the principle of maximum hardness, the even-numbered homotops (Cu₆Zr₇ and Cu₈Zr₅) with larger η are more stable than their adjacent ones. The reason for the variation of chemical hardness with composition is mainly due to the deformation resistance of the electronic density in systems, suggesting the necessity to further investigate the density of states (DOS) to understand the energy and chemical characteristics difference between Cu_xZr_{13-x} clusters.

As the eigenvalue spectra shown in Figure 9, in the smallest clusters Cu₂ and Zr₂, the energy levels are discrete and d and sp peaks are separated. As the cluster size increases, the d and sp levels are broadened. Thus, almost continuous electronic bands are found in Cu_xZr_{13-x} ($3 \leq x \leq 10$). Most importantly, the DOS minimum of both majority manifolds (spin-up) and minority (spin-down) manifolds at the Fermi level are observed for Cu₆Zr₇ and Cu₈Zr₅, corresponding to the energy stability trends discussed above, providing further evidence for the high stability of this cluster. For other components, the Fermi levels cut through the majority or minority manifolds, and some even at the peak position.

It is noteworthy that the atomic structure and electronic structure correlations are expected to give more essential

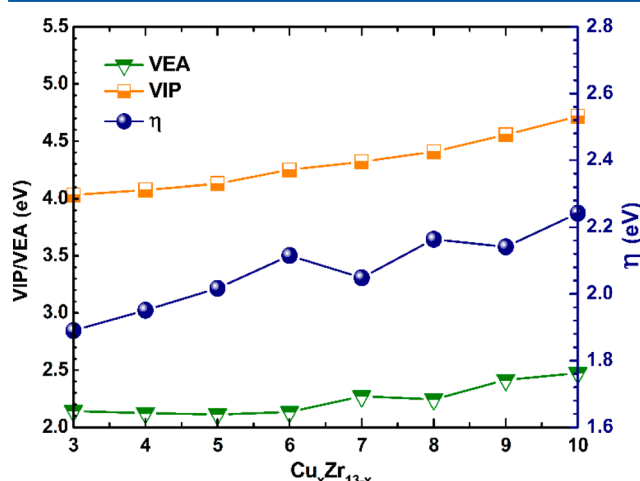


Figure 8. Composition dependence of VIPs (yellow squares), VEAs (green triangles), and chemical hardness, η (navy spheres) of the lowest-energy Cu_xZr_{13-x} ($x = 3-10$) clusters.

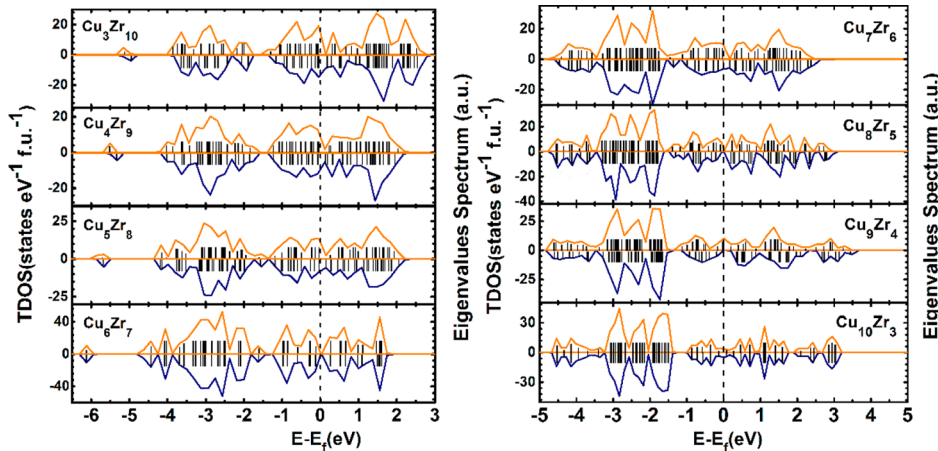


Figure 9. Density of states (DOS) and eigenvalue spectra for $\text{Cu}_x\text{Zr}_{13-x}$ clusters with $3 \leq x \leq 10$. The zero of the energy axes is at the Fermi level. A Gaussian broadening of 0.05 eV is used.

insights into the stability of the metastable glassy materials.^{4,12,15,64–67} Hosokawa⁶⁸ performed photoemission experiments to understand the superior GFA of the $\text{Pd}_{40}\text{Ni}_{40}\text{P}_{20}$ ternary MGs, which showed remarkably lower density of states (DOS) at the Fermi surface, E_F , when compared to the cases of bulk Ni or bulk Pd. Nagel and Tauc¹⁵ proposed a nearly free-electron model for understanding electronic behaviors in MGs. They suggested the decrease in DOS at the Fermi surface to be a criterion for excellent GFA. In our studies, the Cu_6Zr_7 and Cu_8Zr_5 clusters, which are identified to be the dominant clusters of the best glass formers in Cu-Zr BMGs, show both a minimum DOS at the Fermi level and the high chemical hardness, strongly supporting the Nagel-Tauc prediction. The present analysis suggested the close relationship between the icosahedral properties and the glass-forming ability and uncovered the reason for the specially stable icosahedral clusters prevail in Cu-Zr BMGs.

4. CONCLUSIONS

In our study, the first-principles approach combined with molecular dynamics (MD) simulations are used to explain the experimental observation that the best glass formers of Cu-Zr BMGs are specifically located at the compositions of $\text{Cu}_{50}\text{Zr}_{50}$ and $\text{Cu}_{64}\text{Zr}_{36}$. Through the systematically statistical analysis of $\text{Cu}_x\text{Zr}_{100-x}$ ($45 \leq x \leq 70$) alloys by MD simulations, weak but significant peaks of the fraction of Cu_6Zr_7 and Cu_8Zr_5 icosahedral clusters showed up in $\text{Cu}_{50}\text{Zr}_{50}$ and $\text{Cu}_{64}\text{Zr}_{36}$, respectively. The nature of the basic polyhedra impact on GFA is further characterized by first-principles calculations along with CE techniques. The Cu_6Zr_7 and Cu_8Zr_5 clusters are found to have the lowest formation energy among the icosahedral clusters of $\text{Cu}_x\text{Zr}_{13-x}$ ($3 \leq x \leq 10$), as well as sharing some common specialties in electronic structure and chemical hardness, indicating that the stability of local icosahedral clusters greatly correlated to the glass-forming ability. This study suggested a link between the compositional location of the best glass formers and their basic orders, suggesting the strong dependence of the icosahedral properties on the formation of improved metallic glasses.

AUTHOR INFORMATION

Corresponding Authors

*S.-J. Zhao. E-mail address: shijin.zhao@shu.edu.cn. Tel: 86-21-56331480.

*L.-M. Liu. E-mail address: limin.liu@csrc.ac.cn. Tel: 86-10-82687086.

Notes

The authors declare no competing financial interest.

ACKNOWLEDGMENTS

This work is supported by the National Natural Science Foundation of China (Nos. 51222212 and 50931003), the CAEP foundation (Grant No. 2012B0302052), the MOST of China (973 Project, Grant No. 2011CB922200), the Ministry of Science & Technology of China (Project 2012AA050704), and the 085 Project at Shanghai University. The computation support from the Informalization Construction Project of Chinese Academy of Sciences during the 11th Five-Year Plan Period (No. INFO-115-B01) is also highly acknowledged.

REFERENCES

- (1) Xu, D.; Lohwongwatana, B.; Duan, G.; Johnson, W. L.; Garland, C. Bulk Metallic Glass Formation in Binary Cu-Rich Alloy Series- $\text{Cu}_{100-x}\text{Zr}_x$ ($x = 34, 36, 38.2, 40$ At.%) and Mechanical Properties of Bulk $\text{Cu}_{64}\text{Zr}_{36}$ Glass. *Acta Mater.* **2004**, *52*, 2621–2624.
- (2) Miracle, D. B. A Structural Model for Metallic Glasses. *Nat. Mater.* **2004**, *3*, 697–702.
- (3) Ma, D.; Stoica, A. D.; Wang, X. L. Power-Law Scaling and Fractal Nature of Medium-Range Order in Metallic Glasses. *Nat. Mater.* **2009**, *8*, 30–34.
- (4) Wang, W. H.; Dong, C.; Shek, C. H. Bulk Metallic Glasses. *Mater. Sci. Eng. R.* **2004**, *44*, 45–89.
- (5) Cheng, Y. Q.; Sheng, H. W.; Ma, E. Relationship between Structure, Dynamics, and Mechanical Properties in Metallic Glass-Forming Alloys. *Phys. Rev. B* **2008**, *78*, 014207-1–014207-7.
- (6) Kelton, K. F.; Lee, G. W.; Gangopadhyay, A. K.; Hyers, R. W.; Rathz, T. J.; Rogers, J. R.; Robinson, M. B.; Robinson, D. S. First X-Ray Scattering Studies on Electrostatically Levitated Metallic Liquids: Demonstrated Influence of Local Icosahedral Order on the Nucleation Barrier. *Phys. Rev. Lett.* **2003**, *90*, 195504-1–195504-4.
- (7) Appignanesi, G. A.; Rodríguez Fris, J. A.; Frechero, M. A. Reproducibility of Dynamical Heterogeneities and Metabasin Dynamics in Glass Forming Liquids: The Influence of Structure on Dynamics. *Phys. Rev. Lett.* **2006**, *96*, 237803-1–237803-4.
- (8) Greer, A. L.; Ma, E. Bulk Metallic Glasses: At the Cutting Edge of Metals Research. *MRS Bull.* **2007**, *32*, 611–619.
- (9) Liu, Y. H.; Liu, C. T.; Wang, W. H.; Inoue, A.; Sakurai, T.; Chen, M. W. Thermodynamic Origins of Shear Band Formation and the Universal Scaling Law of Metallic Glass Strength. *Phys. Rev. Lett.* **2009**, *103*, 065504-1–065504-4.

- (10) Guan, P.; Lu, S.; Spector, M. J. B.; Valavalas, P. K.; Falk, M. L. Cavitation in Amorphous Solids. *Phys. Rev. Lett.* **2013**, *110*, 185502-1–185502-5.
- (11) Tang, C.; Harrowell, P. Anomalously Slow Crystal Growth of the Glass-Forming Alloy CuZr. *Nat. Mater.* **2013**, *12*, 507–511.
- (12) Cohen, M. H.; Turnbull, D. Composition Requirements for Glass Formation in Metallic and Ionic Systems. *Nature* **1961**, *189*, 131–132.
- (13) Polk, D. E. The Structure of Glassy Metallic Alloys. *Acta Mater.* **1972**, *20*, 485–491.
- (14) Chen, H. S.; Park, B. K. Role of Chemical Bonding in Metallic Glasses. *Acta Mater.* **1973**, *21*, 395–400.
- (15) Nagel, S. R.; Tauc, J. Nearly-Free-Electron Approach to the Theory of Metallic Glass Alloys. *Phys. Rev. Lett.* **1975**, *35*, 380–383.
- (16) Finney, J. L. Modelling the Structures of Amorphous Metals and Alloys. *Nature* **1977**, *266*, 309–314.
- (17) Lu, Z. P.; Liu, C. T. A New Glass-Forming Ability Criterion for Bulk Metallic Glasses. *Acta Mater.* **2002**, *50*, 3501–3512.
- (18) Lu, Z. P.; Liu, C. T. Glass Formation Criterion for Various Glass-Forming Systems. *Phys. Rev. Lett.* **2003**, *91*, 115505-1–115505-4.
- (19) Mukherjee, S.; Schroers, J.; Johnson, W. L.; Rhim, W. K. Influence of Kinetic and Thermodynamic Factors on the Glass-Forming Ability of Zirconium-Based Bulk Amorphous Alloys. *Phys. Rev. Lett.* **2005**, *94*, 245501-1–245501-4.
- (20) Hirata, A.; Kang, L. J.; Fujita, T.; Klumov, B.; Matsue, K.; Kotani, M.; Yavari, A. R.; Chen, M. W. Geometric Frustration of Icosahedron in Metallic Glasses. *Science* **2013**, *341*, 376–379.
- (21) Wang, D.; Li, Y.; Sun, B. B.; Sui, M. L.; Lu, K.; Ma, E. Bulk Metallic Glass Formation in the Binary Cu-Zr System. *Appl. Phys. Lett.* **2004**, *84*, 4029–4031.
- (22) Sheng, H. W.; Luo, W. K.; Alamgir, F. M.; Bai, J. M.; Ma, E. Atomic Packing and Short-to-Medium-Range Order in Metallic Glasses. *Nature* **2006**, *439*, 419–425.
- (23) Fukuhara, M.; Takahashi, M.; Kawazoe, Y.; Inoue, A. Electronic Rule for Formation of Glassy Alloys. *Appl. Phys. Lett.* **2007**, *90*, 073114-1–073114-3.
- (24) Kaban, I.; Jóvári, P.; Kokotin, V.; Shuleshova, O.; Beuneu, B.; Saksl, K.; Mattern, N.; Eckert, J.; Greer, A. L. Local Atomic Arrangements and Their Topology in Ni-Zr and Cu-Zr Glassy and Crystalline Alloys. *Acta Mater.* **2013**, *61*, 2509–2520.
- (25) Jakse, N.; Pasturel, A. Glass Forming Ability and Short-Range Order in a Binary Bulk Metallic Glass by Ab Initio Molecular Dynamics. *Appl. Phys. Lett.* **2008**, *93*, 113104–113103.
- (26) Almyras, G. A.; Papageorgiou, D. G.; Lekka, C. E.; Mattern, N.; Eckert, J.; Evangelakis, G. A. Atomic Cluster Arrangements in Reverse Monte Carlo and Molecular Dynamics Structural Models of Binary Cu-Zr Metallic Glasses. *Intermetallics* **2011**, *19*, 657–661.
- (27) Tian, H.; Zhang, C.; Wang, L.; Zhao, J.; Dong, C.; Wen, B.; Wang, Q. Ab Initio Molecular Dynamics Simulation of Binary Cu₆₄Zr₃₆ Bulk Metallic Glass: Validation of the Cluster-Plus-Glue-Atom Model. *J. Appl. Phys.* **2011**, *109*, 123520-1–123520-7.
- (28) Mendelev, M. I.; Kramer, M. J.; Ott, R. T.; Sordelet, D. J. Molecular Dynamics Simulation of Diffusion in Supercooled Cu-Zr Alloys. *Philos. Mag.* **2009**, *89*, 109–126.
- (29) Yu, C. Y.; Liu, X. J.; Lu, J.; Zheng, G. P.; Liu, C. T. First-Principles Prediction and Experimental Verification of Glass-Forming Ability in Zr-Cu Binary Metallic Glasses. *Sci. Rep.* **2013**, *3*, 2124-1–2124-5.
- (30) Yang, L.; et al. Design of Cu₈Zr₅-Based Bulk Metallic Glasses. *Appl. Phys. Lett.* **2006**, *88*, 241913-1–241913-3.
- (31) Wang, X. D.; Yin, S.; Cao, Q. P.; Jiang, J. Z.; Franz, H.; Jin, Z. H. Atomic Structure of Binary Cu_{64.5}Zr_{35.5} Bulk Metallic Glass. *Appl. Phys. Lett.* **2008**, *92*, 011902-1–011902-3.
- (32) Tang, M. B.; Zhao, D. Q.; Pan, M. X.; Wang, W. H. Binary Cu-Zr Bulk Metallic Glasses. *Chin. Phys. Lett.* **2004**, *21*, 901–903.
- (33) Xia, J.; Qiang, J.; Wang, Y.; Wang, Q.; Dong, C. Ternary Bulk Metallic Glasses Formed by Minor Alloying of Cu₈Zr₅ Icosahedron. *Appl. Phys. Lett.* **2006**, *88*, 101907-1–101907-3.
- (34) Li, Y.; Guo, Q.; Kalb, J. A.; Thompson, C. V. Matching Glass-Forming Ability with the Density of the Amorphous Phase. *Science* **2008**, *322*, 1816–1819.
- (35) Bendert, J. C.; Gangopadhyay, A. K.; Mauro, N. A.; Kelton, K. F. Volume Expansion Measurements in Metallic Liquids and Their Relation to Fragility and Glass Forming Ability: An Energy Landscape Interpretation. *Phys. Rev. Lett.* **2012**, *109*, 185901-1–185901-5.
- (36) Ward, L.; Miracle, D.; Windl, W.; Senkov, O. N.; Flores, K. Structural Evolution and Kinetics in Cu-Zr Metallic Liquids from Molecular Dynamics Simulations. *Phys. Rev. B* **2013**, *88*, 134205-1–134205-10.
- (37) Plimpton, S. Fast Parallel Algorithms for Short-Range Molecular Dynamics. *J. Comput. Phys.* **1995**, *117*, 1–19.
- (38) Blöchl, P. E. Projector Augmented-Wave Method. *Phys. Rev. B* **1994**, *50*, 17953–17979.
- (39) Perdew, J. P.; Burke, K.; Ernzerhof, M. Generalized Gradient Approximation Made Simple. *Phys. Rev. Lett.* **1996**, *77*, 3865–3868.
- (40) Kresse, G.; Furthmüller, J. Efficient Iterative Schemes for Ab Initio Total-Energy Calculations Using a Plane-Wave Basis Set. *Phys. Rev. B* **1996**, *54*, 11169–11186.
- (41) van de Walle, A.; Asta, M.; Ceder, G. The Alloy Theoretic Automated Toolkit: A User Guide. *Calphad* **2002**, *26*, 539–553.
- (42) Ferreira, L. G.; Wei, S.-H.; Zunger, A. First-Principles Calculation of Alloy Phase Diagrams: The Renormalized-Interaction Approach. *Phys. Rev. B* **1989**, *40*, 3197–3231.
- (43) Saracibar, A.; Van der Ven, A.; Arroyo-de Dompablo, M. E. Crystal Structure, Energetics, and Electrochemistry of Li₂FeSiO₄ Polymorphs from First Principles Calculations. *Chem. Mater.* **2012**, *24*, 495–503.
- (44) Taylor, K. J.; Pettiette-Hall, C. L.; Cheshnovsky, O.; Smalley, R. E. Ultraviolet Photoelectron Spectra of Coinage Metal Clusters. *J. Chem. Phys.* **1992**, *96*, 3319–3329.
- (45) Chang, C. M.; Chou, M. Y. Alternative Low-Symmetry Structure for 13-Atom Metal Clusters. *Phys. Rev. Lett.* **2004**, *93*, 133401-1–133401-4.
- (46) Fernández, E. M.; Soler, J. M.; Garzón, I. L.; Balbás, L. C. Trends in the Structure and Bonding of Noble Metal Clusters. *Phys. Rev. B* **2004**, *70*, 165403-1–165403-14.
- (47) Piotrowski, M. J.; Piquini, P.; Da Silva, J. L. F. Density Functional Theory Investigation of 3d, 4d, and 5d 13-Atom Metal Clusters. *Phys. Rev. B* **2010**, *81*, 155446-1–155446-14.
- (48) Rycroft, C. H.; Grest, G. S.; Landry, J. W.; Bazant, M. Z. Analysis of Granular Flow in a Pebble-Bed Nuclear Reactor. *Phys. Rev. E* **2006**, *74*, 021306-1–021306-16.
- (49) Li, M.; Wang, C. Z.; Hao, S. G.; Kramer, M. J.; Ho, K. M. Structural Heterogeneity and Medium-Range Order in Zr_xCu_{100-x} Metallic Glasses. *Phys. Rev. B* **2009**, *80*, 184201-1–184201-7.
- (50) Xia, J. H.; Qiang, J.; Wang, Y.; Wang, Q.; Dong, C. Ternary Bulk Metallic Glasses Formed by Minor Alloying of Cu₈Zr₅ Icosahedron. *Appl. Phys. Lett.* **2006**, *88*, 101907-1–101907-3.
- (51) Lekka, C. E.; Ibenskas, A.; Yavari, A. R.; Evangelakis, G. A. Tensile Deformation Accommodation in Microscopic Metallic Glasses Via Subnanocluster Reconstructions. *Appl. Phys. Lett.* **2007**, *91*, 214103-1–214103-3.
- (52) Wang, Q.; Dong, C.; Qiang, J.; Wang, Y. Cluster Line Criterion and Cu-Zr-Al Bulk Metallic Glass Formation. *Mater. Sci. Eng., A* **2007**, *449*–451, 18–23.
- (53) Jellinek, J.; Krissinel, E. B. Ni_nAl_m Alloy Clusters: Analysis of Structural Forms and Their Energy Ordering. *Chem. Phys. Lett.* **1996**, *258*, 283–292.
- (54) Krissinel, E. B.; Jellinek, J. 13-Atom Ni-Al Alloy Clusters: Structures and Dynamics. *Int. J. Quantum Chem.* **1997**, *62*, 185–197.
- (55) Van der Ven, A.; Thomas, J. C.; Xu, Q. C.; Swoboda, B.; Morgan, D. Nondilute Diffusion from First Principles: Li Diffusion in Li_xTiS₂. *Phys. Rev. B* **2008**, *78*, 104306-1–104306-12.
- (56) Takeuchi, A.; Inoue, A. Calculations of Amorphous-Forming Composition Range for Ternary Alloy Systems and Analyses of Stabilization of Amorphous Phase and Amorphous-Forming Ability. *Mater. Trans.* **2001**, *42*, 1435–1444.

- (57) Shindo, T.; Waseda, Y.; Inoue, A. Prediction of Glass-Forming Composition Ranges in Zr-Ni-Al Alloys. *Mater. Trans.* **2002**, *43*, 2502–2508.
- (58) Guo, H.; Yan, P. F.; Wang, Y. B.; Tan, J.; Zhang, Z. F.; Sui, M. L.; Ma, E. Tensile Ductility and Necking of Metallic Glass. *Nat. Mater.* **2007**, *6*, 735–739.
- (59) Luo, W. K.; Sheng, H. W.; Alamgir, F. M.; Bai, J. M.; He, J. H.; Ma, E. Icosahedral Short-Range Order in Amorphous Alloys. *Phys. Rev. Lett.* **2004**, *92*, 145502-1–145502-4.
- (60) Lund, A. C.; Schuh, C. A. Yield Surface of a Simulated Metallic Glass. *Acta Mater.* **2003**, *51*, 5399–5411.
- (61) Parr, R. G.; Pearson, R. G. Absolute Hardness: Companion Parameter to Absolute Electronegativity. *J. Am. Chem. Soc.* **1983**, *105*, 7512–7516.
- (62) Parr, R. G.; Chattaraj, P. K. Principle of Maximum Hardness. *J. Am. Chem. Soc.* **1991**, *113*, 1854–1855.
- (63) Parr, R. G.; Yang, W. *Density-Functional Theory of Atoms and Molecules*; Oxford University Press: 1989; Vol. 16.
- (64) Häussler, P. Interrelations between Atomic and Electronic Structures-Liquid and Amorphous Metals as Model Systems. *Phys. Rep.* **1992**, *222*, 65–143.
- (65) Greer, A. L. Confusion by Design. *Nature* **1993**, *366*, 303–304.
- (66) Wang, W. H. Roles of Minor Additions in Formation and Properties of Bulk Metallic Glasses. *Prog. Mater. Sci.* **2007**, *52*, 540–596.
- (67) Ma, D.; Stoica, A. D.; Wang, X. L. Power-Law Scaling and Fractal Nature of Medium-Range Order in Metallic Glasses. *Nat. Mater.* **2009**, *8*, 30–34.
- (68) Hosokawa, S.; Hoppo, N.; Sato, H.; Taniguchi, M.; Ichitsubo, T.; Sakurai, M.; Matsubara, E.; Nishiyama, N. Incident Photon-Energy Dependence of the Electronic Density of States in $Pd_{42.5}Ni_{7.5}Cu_{30}P_{20}$ Metallic Glass. *Mater. Trans.* **2005**, *46*, 2803–2806.